Simulation of Semiconductor Devices Using a Galerkin/Spherical Harmonic Expansion Approach to Solving the Coupled Poisson-Boltzmann System

Khalid Rahmat, *Member, IEEE*, Jacob White, *Member, IEEE*, and Dimitri A. Antoniadis, *Fellow, IEEE*

***Abstract*—This paper describes a Galerkin/spherical harmonics approach for solving the coupled Poisson-Boltzmann system of equations for the electron distribution function and the electric potential, which can then be used to calculate other parameters of interest such as current flow and electron temperature. The Galerkin approach described here has some pragmatic advantages in space-dependent problems over more commonly used term-matching techniques for arbitrary order spherical harmonic expansions in momentum space, but the method requires a careful treatment of the boundary conditions and upwinded discretization methods. Results are presented for nonuniformly doped one-dimensional devices using up to third order spherical harmonics to show the importance of including higher order harmonics to accurately calculate the distribution function in high field regions.**

I. Introduction

THE DIRECT solution of the Boltzmann equation for modeling transport in semiconductors has been pursued for over two decades, and many ingenious techniques have been developed for this purpose. These include an integral equation method [1], the Monte Carlo method [2], a number of methods using different basis function expansions [3], [4], and direct integration [5]. The most commonly used of these techniques is the Monte Carlo method, primarily because the method's flexibility allows details such as complicated band structures and scattering mechanisms to be easily incorporated. The main disadvantage of the Monte Carlo method is its computational expense, especially when attempting to reduce the statistical noise in the low density tails of the distribution function.

As an alternative to the Monte Carlo method for the solution of the Boltzmann equation, we shall consider the spherical harmonic expansion method. Earlier work on this method has shown its viability for low order expansions [6], [7]. Results using very high order expansions have been reported for the homogeneous case [8], but simulations of inhomogeneous problems in one or two-dimensions have used only zero- and first-order spherical harmonic expansions. Approaches to including higher order expansions in spatially dependent problems were described formally in [9] and more recently in [8], but the related implementation and associated numerical issues were not a primary focus. In particular, computational results demonstrating the importance of higher-order spherical harmonic expansions for spatially dependent problems have not been presented.

In this paper we describe a Galerkin approach to solving the coupled Poisson-Boltzmann equation with arbitrary-order spherical harmonic expansions, and use the method to demonstrate the importance of higher-order spherical harmonic expansions for one-dimensional (1-D) spatially dependent problems. Our specific Galerkin approach differs somewhat from the term-matching approaches described in [9] and [8]. In our approach, the Boltzmann equation is first discretized in physical space using a finite-difference method, and then the spherical harmonics expansion is used to solve the generated large system of partial differential equations in k-space. This approach makes it easier to implement simulation programs for space-dependent problems using arbitrary order spherical harmonic expansions, but the approach is not without a cost. The physical-space finite-difference discretization must be upwinded in a conservative way to insure current conservation and stability. In addition, the boundary conditions must be considered with care.

The next section provides some background and a review of earlier work using the spherical harmonics approach. Then in Section III our contribution in extending this technique to arbitrary order using a Galerkin method is explained. The numerical difficulties encountered and their resolution for one space dimension problems are described in Section IV. Finally, in Section V, results using the arbitrary order approach for the test case of an n^+nn^+ diode will be discussed and compared with the results using a hydrodynamics based model.

Manuscript received August 16, 1995; revised January 30, 1996 and June 24, 1996. This work was supported by Hewlett-Packard and by ARPA under ONR Contract N00174-93-C-0035. This paper was recommended by Associate Editor S. Duvall.

K. Rahmat was with the Research Laboratory of Electronics, Department of Electrical Engineering and Computer Science, Massachusetts Institute of Technology, Cambridge, MA 02139 USA. He is now with Hewlett-Packard Laboratories, Hewlett-Packard Co., Palo Alto, CA 94304 USA.

J. White and D. Antoniadis are with the Research Laboratory of Electronics, Department of Electrical Engineering and Computer Science, Massachusetts Institute of Technology, Cambridge, MA 02139 USA.

Publisher Item Identifier S 0278-0070(96)07396-4.

0278–0070/96$05.00 © 1996 IEEE

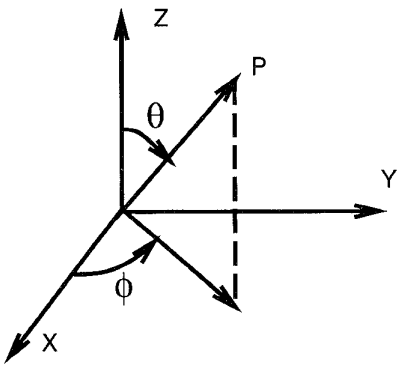

Fig. 1. The coordinate system used in the spherical harmonic expansion.

II. The Spherical Harmonic Expansion of the Boltzmann Equation

Due to the spherical symmetry of the band structure and the randomizing nature of most scattering processes, one can expect the distribution function to have some degree of spherical symmetry in momentum space. Note also that the equilibrium distribution, which is a Maxwellian for the nondegenerate case, is spherically symmetric. Thus, a basis function expansion of the distribution function should exploit this symmetry. Consequently, a plausible choice for the basis functions are the surface spherical harmonics denoted by $Y_{lm}(\theta,\phi)$, in which case the distribution function can be expressed as (see Fig. 1)

$$f(\boldsymbol{r},\boldsymbol{k}) = \sum_{lm} f_{lm}(\boldsymbol{r},k) Y_{lm}(\theta,\phi) \tag{1}$$

where $k = |\boldsymbol{k}|$ is the magnitude of the momentum and f_{lm} are the spherical harmonic coefficients. The expansion in (1) implies that at each real space point $\boldsymbol{r}$, the momentum space description of the distribution function is specified on each sphere of radius k by a weighted sum of surface spherical harmonics. The weight of each harmonic, Y_{lm}, is specified by f_{lm}. The essence of the problem is to find these weights on as many spheres in momentum space as desired. Of course, this choice for the expansion will be efficient only if few spherical harmonics are needed to accurately represent the momentum space distribution.

It can be helpful to note that the coefficients of the low-order spherical harmonics correspond to basic physical quantities. The lowest order harmonic coefficient, $f_{0,0}$, provides information about the isotropic part of the distribution. The integral of $f_{0,0}$ over all momentum space yields the electron concentration at each real space point. The first order harmonic describes the asymmetry of the distribution in the direction of the applied field and the integral of $f_{1,0}$, after multiplication by the electron velocity, yields the current.

The standard approach to solving for the expansion coefficients is to first substitute (1) into the Boltzmann equation

$$\begin{aligned} \boldsymbol{v}(\boldsymbol{k})\nabla_{\boldsymbol{r}} f(\boldsymbol{r},\boldsymbol{k}) - \frac{q\mathcal{E}(\boldsymbol{r})}{\hbar}\cdot\nabla_{\boldsymbol{k}} f(\boldsymbol{r},\boldsymbol{k}) \\ = \int S(\boldsymbol{r},\boldsymbol{k}',\boldsymbol{k}) f(\boldsymbol{r},\boldsymbol{k}')\, d^3\boldsymbol{k}' - f(\boldsymbol{r},\boldsymbol{k}) \\ \cdot \int S(\boldsymbol{r},\boldsymbol{k},\boldsymbol{k}')\, d^3\boldsymbol{k}', \end{aligned} \tag{2}$$

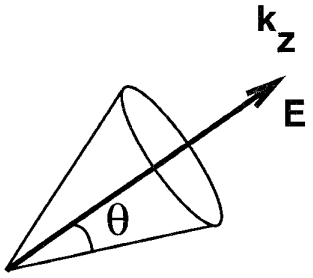

Fig. 2. Coordinate system for the 1-D real space problem.

where $\boldsymbol{v}(\boldsymbol{k})$ is the electron velocity, $\mathcal{E}$ is the applied electric field, q is the electron charge, and $S(\boldsymbol{r},\boldsymbol{k}',\boldsymbol{k})$ is the scattering rate from momentum $\boldsymbol{k}'$ to $\boldsymbol{k}$ at real space position $\boldsymbol{r}$. The combined equation is then used to generate a set of coupled partial differential equation in the expansion coefficients [4], [9]. This set of partial differential equations is then solved by introducing a discretization method to generate an algebraic equation system for the desired set of coefficients f_{lm}.

For modeling transport in one real space dimension, z, and assuming a z-directed electric field, the associated two-dimensional (2–D) momentum space can be represented in polar coordinates $k = |\boldsymbol{k}|$ and $\theta = \arccos(\boldsymbol{k}\cdot\boldsymbol{k_z}/|\boldsymbol{k}|\,|\boldsymbol{k_z}|)$, as shown in Fig. 2. Then, the distribution function can be expanded in Legendre polynomials of the angle θ:

$$f(z,\boldsymbol{k}) = \sum f_n(z,k) P_n(\cos\theta) \tag{3}$$

where P_n is the nth order Legendre polynomial. In the subsections below, we use the expansion in (3) for the distribution function, f, in each term of the Boltzmann Transport Equation (BTE).

A. The Diffusion Term: $\boldsymbol{v}(\boldsymbol{k})\cdot\nabla_{\boldsymbol{r}} f(\boldsymbol{r},\boldsymbol{k})$

The velocity $\boldsymbol{v}(\boldsymbol{k})$ is determined from the band structure: $\boldsymbol{v}(\boldsymbol{k}) = (1/\hbar)(\partial E/\partial\boldsymbol{k})$, which is assumed to be spherically symmetric and described by a relation of the form: $\gamma(E) = \hbar^2k^2/2m^* = \hbar^2\boldsymbol{k}\cdot\boldsymbol{k}/2m^*$. This allows for a nonparabolic band structure by using an appropriate form for $\gamma(E)$. Of course, $\gamma(E) = E$ leads to the familiar parabolic band model. Thus, $\boldsymbol{v}(\boldsymbol{k})$ is given by

$$\boldsymbol{v}(\boldsymbol{k}) = \left(\frac{2\gamma}{m^*}\right)^{1/2}\frac{dE}{d\gamma}\boldsymbol{i}_k = v(k)\boldsymbol{i}_k. \tag{4}$$

where $\boldsymbol{i}_k$ is the unit vector in the radial $\boldsymbol{k}$ direction. Note that the magnitude of the velocity is purely a function of the energy and its direction is always radial. Using the above expression for the velocity, the diffusion term in one real space dimension becomes

$$\begin{aligned} \boldsymbol{v}(\boldsymbol{k})\cdot\nabla_{\boldsymbol{r}} f(\boldsymbol{r},\boldsymbol{k}) &= \boldsymbol{v}(\boldsymbol{k})\cdot\frac{\partial f}{\partial z}\boldsymbol{i}_z \\ &= v(k)\boldsymbol{i}_k\cdot\frac{\partial}{\partial z}\left[\sum f_n(z,k)P_n(\cos\theta)\right]\boldsymbol{i}_z. \end{aligned} \tag{5}$$

The scalar product above can be evaluated by projecting the radial $\boldsymbol{i}_k$ vector onto the z-axis which evaluates to $\cos\theta$,

whence, the diffusion term becomes:

$$\boldsymbol{v}(\boldsymbol{k}) \cdot \nabla_{\boldsymbol{r}} f(\boldsymbol{r}, \boldsymbol{k}) = v(k) \cos\theta \left[\sum \frac{\partial f_n(z,k)}{\partial z} P_n(\cos\theta) \right]. \tag{6}$$

Using the following identity for Legendre polynomials [10]:

$$xP_n(x) = \frac{(n+1)P_{n+1}(x) + nP_{n-1}(x)}{2n+1} \tag{7}$$

the diffusion term can be written as

$$\boldsymbol{v}(\boldsymbol{k}) \nabla_{\boldsymbol{r}} f(\boldsymbol{r}, \boldsymbol{k}) = v(k) \sum \frac{\partial f_n(z,k)}{\partial z} \cdot \left(\frac{(n+1)P_{n+1}(\cos\theta) + nP_{n-1}(\cos\theta)}{2n+1} \right). \tag{8}$$

B. The Drift Term: $q\mathcal{E}(\boldsymbol{r})/\hbar \cdot \nabla_{\boldsymbol{k}} f(\boldsymbol{r}, \boldsymbol{k})$

Again assuming one real space direction, chosen to be z, $f(\boldsymbol{r}, \boldsymbol{k})$ can be replaced by $f(z, \boldsymbol{k})$. In spherical coordinates, the gradient of any function $h(k, \theta)$ which has no ϕ dependence is

$$\nabla_{\boldsymbol{k}} h(\boldsymbol{k}) = \frac{\partial h(k,\theta)}{\partial k} \boldsymbol{i}_k + \frac{1}{k} \frac{\partial h(k,\theta)}{\partial \theta} \boldsymbol{i}_\theta. \tag{9}$$

Hence, the gradient of f with respect to the $\boldsymbol{k}$ vector can be explicitly written as

$$\begin{aligned} \nabla_{\boldsymbol{k}} f(\boldsymbol{r}, \boldsymbol{k}) &= \nabla_{\boldsymbol{k}} \sum f_n(z,k) P_n(\cos\theta) \\ &= \sum \frac{\partial f_n(z,k)}{\partial k} P_n(\cos\theta) \boldsymbol{i}_k \\ &\quad + \sum \frac{f_n(z,k)}{k} \frac{\partial P_n(\cos\theta)}{\partial \theta} \boldsymbol{i}_\theta \\ &= \sum \frac{\partial f_n(z,k)}{\partial k} P_n(\cos\theta) \boldsymbol{i}_k \\ &\quad + \sum \left(\frac{f_n(z,k)}{k} \frac{\partial P_n(\cos\theta)}{\partial(\cos\theta)} (-\sin\theta) \right) \boldsymbol{i}_\theta \end{aligned} \tag{10}$$

where there is no ϕ dependence of the distribution function due to its symmetry about the z-directed electric field. The scalar product of the gradient vector with the z-directed electric field can be determined by projecting the gradient onto the z-axis. For any vector of the form $f_r \boldsymbol{i}_{\boldsymbol{r}} + f_\theta \boldsymbol{i}_\theta$, the projection onto the z-axis is $f_r \cos\theta - f_\theta \sin\theta$. Therefore,

$$\begin{aligned} &\frac{q\mathcal{E}(\boldsymbol{r})}{\hbar} \cdot \nabla_{\boldsymbol{k}} f(\boldsymbol{r}, \boldsymbol{k}) \\ &\quad = \frac{q\mathcal{E}(z)}{\hbar} \left[\sum \frac{\partial f_n(z,k)}{\partial k} P_n(\cos\theta) \cos\theta \right. \\ &\qquad \left. + \sum \frac{f_n(z,k)}{k} \frac{\partial P_n(\cos\theta)}{\partial(\cos\theta)} \sin^2\theta \right]. \end{aligned} \tag{11}$$

The identity [10]

$$(x^2 - 1) P_n'(x) = nxP_n(x) - nP_{n-1}(x) \tag{12}$$

together with (7) yields

$$(x^2 - 1) P_n'(x) = \frac{n(n+1)P_{n+1}(x) - n(n+1)P_{n-1}(x)}{2n+1} \tag{13}$$

where $P_n'(x)$ is the derivative of $P_n(x)$ with respect to x. Using (13), the drift term can then be written as

$$\begin{aligned} &\frac{q\mathcal{E}(z)}{\hbar} \left[\sum \frac{\partial f_n(z,k)}{\partial k} \left(\frac{(n+1)P_{n+1}(x) + nP_{n-1}(x)}{2n+1} \right) \right. \\ &\quad \left. - \sum \frac{f_n(z,k)}{k} \left(\frac{n(n+1)P_{n+1}(x) - n(n+1)P_{n-1}(x)}{2n+1} \right) \right] \end{aligned} \tag{14}$$

where $x \equiv \cos\theta$ for notational convenience. Rewriting the above equation to factor out the Legendre polynomials gives

$$\begin{aligned} &\frac{q\mathcal{E}(\boldsymbol{r})}{\hbar} \cdot \nabla_{\boldsymbol{k}} f(\boldsymbol{r}, \boldsymbol{k}) \\ &\quad = \frac{q\mathcal{E}(z)}{\hbar} \left[\sum \frac{1}{2n+1} \left(n \frac{\partial f_n(z,k)}{\partial k} + n(n+1) \frac{f_n(z,k)}{k} \right) \right. \\ &\qquad \cdot P_{n-1}(x) + \sum \frac{1}{2n+1} \\ &\qquad \left. \cdot \left((n+1) \frac{\partial f_n(z,k)}{\partial k} - n(n+1) \frac{f_n(z,k)}{k} \right) P_{n+1}(x) \right]. \end{aligned} \tag{15}$$

C. Complete BTE Expansion in Legendre Polynomials

To rewrite (15) in terms of the energy requires the following identity, derived from (4),

$$\frac{1}{\hbar} \frac{\partial f_n(z,k)}{\partial k} = \frac{\partial f_n(z,E)}{\partial E} v(E) \tag{16}$$

$$\frac{1}{v(E)} \left(\frac{1}{\hbar} \frac{f_n(z,k)}{k} \right) = f_n(z,E) \frac{\gamma'}{2\gamma} \tag{17}$$

where $\gamma' \equiv d\gamma/dE$. The diffusion term is nearly unchanged under this change of variables as it contains no explicit dependence on the momentum or energy vector,

$$\begin{aligned} &\boldsymbol{v}(\boldsymbol{k}) \cdot \nabla_{\boldsymbol{r}} f(\boldsymbol{r}, \boldsymbol{k}) \\ &\quad = v(E) \sum \frac{\partial f_n(z,E)}{\partial z} \\ &\qquad \cdot \left[\frac{(n+1)P_{n+1}(\cos\theta) + nP_{n-1}(\cos\theta)}{2n+1} \right]. \end{aligned} \tag{18}$$

The drift term (15) becomes

$$\begin{aligned} &\frac{q\mathcal{E}(\boldsymbol{r})}{\hbar} \cdot \nabla_{\boldsymbol{k}} f(\boldsymbol{r}, \boldsymbol{k}) \\ &\quad = q\mathcal{E}(z) v(E) \left[\sum \frac{1}{2n+1} \right. \\ &\qquad \cdot \left(n \frac{\partial f_n(z,E)}{\partial E} + \frac{n(n+1)\gamma'}{2\gamma} f_n(z,E) \right) \\ &\qquad \cdot P_{n-1}(x) + \sum \frac{1}{2n+1} \\ &\qquad \cdot \left((n+1) \frac{\partial f_n(z,E)}{\partial E} - \frac{n(n+1)\gamma'}{2\gamma} f_n(z,E) \right) \\ &\qquad \left. \cdot P_{n+1}(x) \right]. \end{aligned} \tag{19}$$

The sum of the above two expressions forms the left-hand side of the Boltzmann equation. The coefficient for the nth

Legendre polynomial is therefore given as:

$$\sum v(E)\left[\left(\frac{n}{2n-1}\frac{\partial f_{n-1}}{\partial z}+\frac{n+1}{2n+3}\frac{\partial f_{n+1}}{\partial z}\right)\right.$$
$$-q\mathcal{E}\left(\frac{n}{2n-1}\frac{\partial f_{n-1}}{\partial E}+\frac{n+1}{2n+3}\frac{\partial f_{n+1}}{\partial E}\right.$$
$$\left.\left.-\frac{n(n-1)}{2n-1}\frac{\gamma'}{2\gamma}f_{n-1}+\frac{(n+1)(n+2)}{2n+3}\frac{\gamma'}{2\gamma}f_{n+1}\right)\right]$$
$$\cdot P_n(x). \tag{20}$$

The Boltzmann equation can therefore be rewritten as an infinite set of coupled partial differential equations for the spherical harmonic expansion coefficients, one partial differential equation for each order. For example, the partial differential equations generated by the two lowest order expansions are

$n = 0$:

$$\frac{\partial f_1}{\partial z}-q\mathcal{E}\left(\frac{\partial f_1}{\partial E}+\frac{\gamma'}{\gamma}f_1\right)=\frac{3}{v(E)}\left(\frac{\partial f_0}{\partial t}\right)_c \tag{21}$$

$n = 1$:

$$\frac{\partial f_0}{\partial z}+\frac{2}{5}\frac{\partial f_2}{\partial z}-q\mathcal{E}(z)\left(\frac{\partial f_0}{\partial E}+\frac{2}{5}\frac{\partial f_2}{\partial E}+\frac{3}{5}\frac{\gamma'}{\gamma}f_2\right)$$
$$=\frac{1}{v(E)}\left(\frac{\partial f_1}{\partial t}\right)_c. \tag{22}$$

To generate a closed system of equations, all coefficients higher than first-order in (22) can be set to zero, resulting in the equation

$$\frac{\partial f_0}{\partial z}-q\mathcal{E}(z)\left(\frac{\partial f_0}{\partial E}\right)=\frac{1}{v(E)}\left(\frac{\partial f_1}{\partial t}\right)_c. \tag{23}$$

In [7] and [9], (21) and (23) were discretized and, after including appropriate scattering mechanisms, solved for the zeroth-order, f_0 and first order, f_1 coefficients. The results obtained using this technique were satisfactory for the devices and biases studied in [9]. One important question which was not addressed in that earlier work is whether zero and first order expansions are sufficiently accurate for realistic problems. In the next section we present a method which allows for arbitrary order expansions.

III. Arbitrary Order Expansion

In order to examine the impact of including higher order spherical harmonics in the solution of the Boltzmann Equation, it is possible to simply continue the process represented by (21) and (23). That is, one could generate a larger system of coupled partial differential equations, discretize those equations, and then implement the resulting method in a new program. This is essentially the scheme presented in [8] and [9]. A more appealing approach, when examining higher-order effects, is to develop a method in which the number of spherical harmonics can be a program parameter. Use of a Galerkin technique leads to just such a program.

In our Galerkin method, the unknown distribution function is still assumed to be a spherical harmonic expansion with unknown coefficients. Then, instead of generating n partial differential equations in the harmonic coefficients as above, we discretize the Boltzmann equation and multiply the discretized equation in turn by each of the conjugate harmonics and integrate over a sphere in momentum space. This produces a matrix equation for the coefficients of the expansion which accounts for the coupling between spherical harmonics. And since the intermediate step of generating and discretizing partial differential equations for each of the spherical harmonic coefficients is omitted, the approach generalizes easily to arbitrary order.

To begin the Galerkin approach derivation, consider substituting the spherical harmonic expansion into the Boltzmann Equation, multiplying by a conjugate spherical harmonic, and then integrating over a sphere in $\boldsymbol{k}$-space as in

$$\int Y^*_{l'm'}(\theta,\phi)\boldsymbol{v}(\boldsymbol{k})\cdot\frac{\partial}{\partial\boldsymbol{r}}\sum_{lm}f_{lm}(\boldsymbol{r},k)Y_{lm}(\theta,\phi)\,d\Omega$$
$$-\int Y^*_{l'm'}(\theta,\phi)\frac{q\mathcal{E}(\boldsymbol{r})}{\hbar}\cdot\frac{\partial}{\partial\boldsymbol{k}}\sum_{lm}f_{lm}(\boldsymbol{r},k)$$
$$\cdot Y_{lm}(\theta,\phi)\,d\Omega$$
$$=\int Y^*_{l'm'}(\theta,\phi)\mathcal{S}\left(\sum_{lm}f_{lm}(\boldsymbol{r},k)Y_{lm}(\theta,\phi)\right)d\Omega \tag{24}$$

where $\mathcal{S}$ denotes the scattering operator. In the following discussion we develop the Galerkin method in one real space dimension, conventionally chosen to be the z-axis, assuming spherical but not necessarily parabolic bands.

A. The Diffusion Term

In one real space dimension, the first term in (24) is

$$\int Y^*_{l'm'}(\theta,\phi)v(k)\boldsymbol{i}_k\cdot\frac{\partial}{\partial z}\left[\sum_{lm}f_{lm}(z,k)Y_{lm}(\theta,\phi)\right]\boldsymbol{i}_z\,d\Omega \tag{25}$$

where $v(k)$ is given by (4). As the projection of the unit radial $\boldsymbol{i}_k$ vector onto the z-axis is $\cos\theta$, (25) can be rewritten as

$$v(k)\int Y^*_{l'm'}(\theta,\phi)\sum_{lm}\cos\theta\frac{\partial}{\partial z}[f_{lm}(z,k)]Y_{lm}(\theta,\phi)\,d\Omega. \tag{26}$$

Now consider using a two point approximation to the space derivative,

$$\frac{\partial}{\partial z}f_{lm}(z,k)\approx\frac{f^{i+1,j}_{lm}-f^{i,j}_{lm}}{\Delta z} \tag{27}$$

where the i index denotes discretization in space and the j index denotes discretization in energy. Combining (26) and (27), a point (i,j) in the solution space can be written as

$$v(k)\int\sum_{lm}\frac{f^{i+1,j}_{lm}-f^{i,j}_{lm}}{\Delta z}Y^*_{l'm'}(\theta,\phi)Y_{lm}(\theta,\phi)\cos\theta\,d\Omega \tag{28}$$

where $d\Omega=\sin\theta\,d\theta\,d\phi$. Defining

$$G_{l'm';lm}\equiv\int_0^{2\pi}\int_0^{\pi}Y^*_{l'm'}(\theta,\phi)Y_{lm}(\theta,\phi)\cos\theta\sin\theta\,d\theta\,d\phi \tag{29}$$

then the discretized diffusion term of the BTE can be written as

$$v^j \sum_{lm} \frac{f_{lm}^{i+1,j} - f_{lm}^{i,j}}{\Delta z} G_{l'm';lm} \tag{30}$$

where v^j is the magnitude of the velocity vector. More compactly,

$$\frac{v^j}{\Delta z} G(f^{i+1,j} - f^{i,j}) \tag{31}$$

where f is the vector of coefficients and G is the matrix defined by (29). One advantage of writing the diffusion term in this compact form is that it clearly shows the coupling between the different coefficients in the expansion. Note that G represents the coupling between harmonics at a particular point in real space whereas the approximation to $\partial/\partial z$ represents the coupling between two points in real space for a particular harmonic.

B. The Drift Term

After substituting the spherical harmonic expansion for the distribution, performing the scalar product with the electric field, and multiplying by the conjugate harmonics, the drift term can be written as

$$-\int Y_{l'm'}^*(\theta,\phi) \frac{q\mathcal{E}(z)}{\hbar} \sum_{lm} \left[\frac{\partial f_{lm}(z,k)}{\partial k} Y_{lm}(\theta,\phi) \cos\theta - \frac{f_{lm}(z,k)}{k} \frac{\partial Y_{lm}(\theta,\phi)}{\partial \theta} \sin\theta \right] d\Omega. \tag{32}$$

Moving the electric field outside the integral and reorganizing the expression as a sum of two integrals over Ω yields

$$\frac{-q\mathcal{E}(z)}{\hbar} \int \sum_{lm} \left[\frac{\partial f_{lm}(z,k)}{\partial k} Y_{l'm'}^*(\theta,\phi) Y_{lm}(\theta,\phi) \cos\theta - \frac{f_{lm}(z,k)}{k} Y_{l'm'}^*(\theta,\phi) \frac{\partial Y_{lm}(\theta,\phi)}{\partial \theta} \sin\theta \right] d\Omega. \tag{33}$$

We can then approximate the derivative with respect to the magnitude of the $\boldsymbol{k}$ vector or energy as a difference

$$\frac{\partial}{\partial k}[f_{lm}(z,k)] = \frac{\partial}{\partial E}[f_{lm}(z,E)]\hbar v(E) \approx \hbar v^j \left[\frac{f_{lm}^{i,j+1} - f_{lm}^{i,j}}{\Delta E} \right]. \tag{34}$$

where (16) was used to change variables from the magnitude of the $\boldsymbol{k}$ vector to energy, and v^j denotes $v(E^j)$. With these substitutions, and the relation in (17), the drift term is

$$-q\mathcal{E}(z)v^j \sum_{lm} \frac{f_{lm}^{i,j+1} - f_{lm}^{i,j+1}}{\Delta E} \iint Y_{l'm'}^*(\theta,\phi) Y_{lm}(\theta,\phi) \cdot \cos\theta \sin\theta \, d\theta \, d\phi + q\mathcal{E}(z)v^j \frac{\gamma' j}{2\gamma^j} \sum_{lm} f_{lm}^{i,j} \iint Y_{l'm'}^*(\theta,\phi) \cdot \frac{\partial Y_{lm}(\theta,\phi)}{\partial \theta} \sin\theta \sin\theta \, d\theta \, d\phi. \tag{35}$$

Note that the first integral was already defined as $G_{l'm';lm}$ in (29). We denote the the second integral as

$$H_{l'm';lm} = \int_0^{2\pi} \int_0^{\pi} Y_{l'm'}^*(\theta,\phi) \frac{\partial Y_{lm}(\theta,\phi)}{\partial \theta} \sin\theta \sin\theta \, d\theta \, d\phi \tag{36}$$

which results in a compact form for the drift term,

$$-q\mathcal{E}\frac{v^j}{\Delta E} G(f^{i,j+1} - f^{i,j}) + q\mathcal{E}\frac{v^j \gamma'^j}{2\gamma^j} H f^{i,j}. \tag{37}$$

C. The Complete Equation

The final task is to put the above expression in a matrix form. First we introduce some more notation to simplify the final form. Let

$$\begin{aligned} a^{i,j} &= \frac{q\mathcal{E}^i}{\Delta E} v^j \\ b^{i,j} &= \frac{q\mathcal{E}^i \gamma'^j}{2\gamma^j} v^j \\ c^{i,j} &= \frac{v^j}{\Delta z} \end{aligned} \tag{38}$$

and

$$\begin{aligned} W_1^{i,j} &= (-c^{i,j} + a^{i,j})G + b^{i,j}H \\ W_2^{i,j} &= c^{i,j}G \\ W_3^{i,j} &= -a^{i,j}G. \end{aligned} \tag{39}$$

Then the left-hand side of the Boltzmann equation, in terms of the spherical harmonic coefficients, can be written in matrix form as

$$\begin{bmatrix} \ddots & \ddots & & \ddots & & & \mathbf{0} \\ & W_1^{i,j} & W_2^{i,j} & & W_3^{i,j} & & \\ & & W_1^{i+1,j} & W_2^{i+1,j} & & W_3^{i+1,j} & \\ & & \ddots & \ddots & & & \ddots \\ & \mathbf{0} & & & & \mathbf{0} & \end{bmatrix} \cdot \begin{bmatrix} \vdots \\ f^{i,j} \\ f^{i+1,j} \\ \vdots \\ f^{i,j+1} \\ f^{i+1,j+1} \\ \vdots \end{bmatrix}.$$

The right-hand side for the above matrix equation is generated by the scattering terms and the distribution function boundary conditions. Note that the matrix is very sparse—the only off-diagonal nonzero blocks are the ones coupling neighbors in space (W_2) and energy (W_3). The particular location of the blocks depends on the ordering of the unknowns; the above pattern is for a row ordering based on the mesh in Fig. 3.

The order of the expansion enters only through the matrices G, H and the size of the vector f, otherwise the formulation is the same. G and H can be calculated *a priori* for whatever order is needed or they could be computed on the fly as

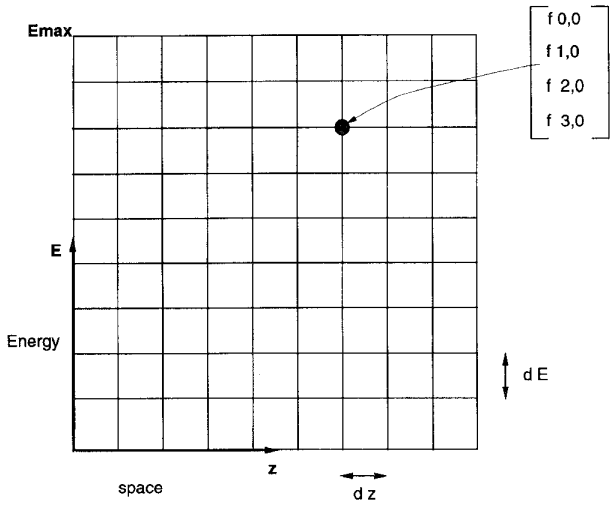

Fig. 3. Mesh used for the 1-D real space problem.

they only involve trigonometric functions which can even be computed numerically if necessary. As an example, up to third order G and H are given below for the 1-D problem

$$G = \begin{bmatrix} 0 & \frac{1}{\sqrt{3}} & 0 & 0 \\ \frac{1}{\sqrt{3}} & 0 & \frac{2}{\sqrt{15}} & 0 \\ 0 & \frac{2}{\sqrt{15}} & 0 & \frac{3}{\sqrt{35}} \\ 0 & 0 & \frac{3}{\sqrt{35}} & 0 \end{bmatrix}$$

$$H = \begin{bmatrix} 0 & -\frac{2}{\sqrt{3}} & 0 & 0 \\ 0 & 0 & -2\sqrt{\frac{3}{5}} & 0 \\ 0 & 2\sqrt{\frac{3}{5}} & 0 & -\frac{12}{\sqrt{35}} \\ 0 & 0 & \frac{6}{\sqrt{35}} & 0 \end{bmatrix}.$$

Although we have assumed a particular form for the discrete approximation to the derivatives in space and energy, the development described above holds equally well for a different discrete approximation, the only change being that the nonzero blocks would be at a different position in the matrix. For example if one used a backward difference for the derivative in space instead of the forward difference used above, then instead of having a nonzero block after the diagonal the nonzero block would be before it.

D. The Scattering Term

We will consider acoustic and optical phonon and ionized impurity scattering; and for all three cases we assume a single spherical band for simplicity. The details of the scattering mechanisms and the parameters used for each are described in the appendix.

1) Acoustic phonon scattering: We will assume that acoustic phonon scattering is isotropic and completely elastic [11]. It can therefore be written as

$$S_{ac}(\boldsymbol{k}, \boldsymbol{k}') = c_{ac}\delta[E(\boldsymbol{k}') - E(\boldsymbol{k})] \tag{40}$$

where c_{ac} is the scattering rate. The net scattering term due to acoustic phonons is

$$\begin{aligned} &\int S_{ac}(\boldsymbol{k}', \boldsymbol{k}) f(\boldsymbol{k}')\, d^3\boldsymbol{k}' - f(\boldsymbol{k}) \int S_{ac}(\boldsymbol{k}, \boldsymbol{k}')\, d^3\boldsymbol{k}' \\ &\quad = c_{ac} \int \delta[E(\boldsymbol{k}) - E(\boldsymbol{k}')] f(\boldsymbol{k}')\, d^3\boldsymbol{k}' - f(\boldsymbol{k}) c_{ac} \\ &\qquad \cdot \int \delta[E(\boldsymbol{k}') - E(\boldsymbol{k})]\, d^3\boldsymbol{k}' \\ &\quad = c_{ac}\left[f_{0,0}Y_{0,0} - \sum_{lm} f_{lm}Y_{lm}(\theta, \phi) \right] g(E) \end{aligned} \tag{41}$$

where $g(E)$ is the density of states which enters due to the change of variables from k to E. Using vector notation the above scattering term up to third order can be written as

$$[Y_{0,0} \quad Y_{1,0} \quad Y_{2,0} \quad Y_{3,0}] \begin{bmatrix} 0 & 0 & 0 & 0 \\ 0 & -1 & 0 & 0 \\ 0 & 0 & -1 & 0 \\ 0 & 0 & 0 & -1 \end{bmatrix} \begin{bmatrix} f_{0,0} \\ f_{1,0} \\ f_{2,0} \\ f_{3,0} \end{bmatrix} \cdot c_{ac}g(E)$$

or more compactly

$$c_{ac}g(E)Y^T S_{ac} f$$

where S_{ac} is understood to be the matrix for the acoustic phonon scattering shown above and Y, f are the vectors of the spherical harmonics and their coefficients, respectively.

The last step is to generate the coefficient matrix by multiplying the conjugate harmonics and integrating over the unit sphere in $\boldsymbol{k}$-space:

$$c_{ac}g(E) \int d\Omega\, Y^* Y^T S_{ac} f$$

2) Optical phonon scattering: The optical phonon scattering rate is given by the expression

$$\begin{aligned} S_{op}(\boldsymbol{k}, \boldsymbol{k}') = c_{op}[&N_{op}\delta(E(\boldsymbol{k}') - E(\boldsymbol{k}) - \hbar\omega) + (N_{op} + 1) \\ &\cdot \delta(E(\boldsymbol{k}') - E(\boldsymbol{k}) + \hbar\omega)] \end{aligned} \tag{42}$$

where $\hbar\omega$ is the energy of the optical phonon and N_{op} the optical phonon number [11]. The net scattering rate due to optical phonons is

$$\begin{aligned} &\int S_{op}(\boldsymbol{k}', \boldsymbol{k}) f(\boldsymbol{k}')\, d^3\boldsymbol{k}' - f(\boldsymbol{k}) \int S_{op}(\boldsymbol{k}, \boldsymbol{k}')\, d^3\boldsymbol{k}' \\ &\quad = c_{op} \int N_{op}\delta[E(\boldsymbol{k}) - E(\boldsymbol{k}') - \hbar\omega] f(\boldsymbol{k}')\, d^3\boldsymbol{k}' + c_{op} \\ &\qquad \cdot \int N_{op}^{+}\delta[E(\boldsymbol{k}) - E(\boldsymbol{k}') + \hbar\omega] f(\boldsymbol{k}')\, d^3\boldsymbol{k}' \\ &\qquad - f(\boldsymbol{k}) c_{op} \int N_{op}\delta[E(\boldsymbol{k}') - E(\boldsymbol{k}) - \hbar\omega]\, d^3\boldsymbol{k}' \\ &\qquad - f(\boldsymbol{k}) c_{op} \int N_{op}^{+}\delta[E(\boldsymbol{k}') - E(\boldsymbol{k}) + \hbar\omega]\, d^3\boldsymbol{k}' \\ &\quad = c_{op}Y_{0,0}[N_{op}f_{0,0}(E - \hbar\omega)g^- + N_{op}^{+}f_{0,0}(E + \hbar\omega)g^+ \\ &\qquad - N_{op}f_{0,0}(E)g^+ - N_{op}^{+}f_{0,0}(E)g^-] \\ &\qquad - \sum_{lm \neq 0} f_{lm}Y_{lm}(\theta, \phi) c_{op}(N_{op}g^+ + N_{op}^{+}g^-) \end{aligned} \tag{43}$$

where $g^- = g(E - \hbar\omega)$, $g^+ = g(E + \hbar\omega)$ are the density of states obtained from the band structure and $N_{op}^{+} = N_{op} + 1$.

In vector notation the above scattering term up to third-order for one real space dimension is

$$c_{op}[Y_{0,0}\quad Y_{1,0}\quad Y_{2,0}\quad Y_{3,0}] \cdot \left(\begin{bmatrix} 1 & 0 & 0 & 0 \\ 0 & 0 & 0 & 0 \\ 0 & 0 & 0 & 0 \\ 0 & 0 & 0 & 0 \end{bmatrix} \begin{bmatrix} f_{0,0}(E+\hbar\omega) \\ f_{1,0}(E+\hbar\omega) \\ f_{2,0}(E+\hbar\omega) \\ f_{3,0}(E+\hbar\omega) \end{bmatrix} (N_{op}^{+} g^{+}) - \begin{bmatrix} 1 & 0 & 0 & 0 \\ 0 & 1 & 0 & 0 \\ 0 & 0 & 1 & 0 \\ 0 & 0 & 0 & 1 \end{bmatrix} \begin{bmatrix} f_{0,0}(E) \\ f_{1,0}(E) \\ f_{2,0}(E) \\ f_{3,0}(E) \end{bmatrix} (N_{op} g^{+} + N_{op}^{+} g^{-}) + \begin{bmatrix} 1 & 0 & 0 & 0 \\ 0 & 0 & 0 & 0 \\ 0 & 0 & 0 & 0 \\ 0 & 0 & 0 & 0 \end{bmatrix} \begin{bmatrix} f_{0,0}(E-\hbar\omega) \\ f_{1,0}(E-\hbar\omega) \\ f_{2,0}(E-\hbar\omega) \\ f_{3,0}(E-\hbar\omega) \end{bmatrix} (N_{op} g^{-}) \right). \tag{44}$$

Note that the scattering rate for the isotropic term depends on energies above and below the energy for which the coefficients are written. If space and energy were discretized and the energy step chosen such that $\hbar\omega$ was a multiple of the energy step then the above scattering rate would couple three different energies, E (with the index j), $E+\hbar\omega$ (with the index $j+l$) and $E-\hbar\omega$ (with the index $j-l$).

D.3 Ionized Impurity Scattering

The scattering operator for ionized impurity scattering in the Brooks-Herring model is [11]

$$S_{\mathrm{BH}}(\boldsymbol{k},\boldsymbol{k}') = \frac{c_{\mathrm{BH}}}{(1+\alpha(1-\cos\theta))}\delta[E(\boldsymbol{k}')-E(\boldsymbol{k})] \tag{45}$$

where θ is the angle between the $\boldsymbol{k}$ and $\boldsymbol{k}'$ vectors and $\alpha = 2k^2/\beta^2$. β is the inverse of the Debye length and therefore depends on the doping concentration; c_{BH} is the scattering rate which depends linearly on the doping concentration. Before we write the scattering integral, we expand the above scattering rate in Legendre polynomials of $\cos\theta$ (as there is no ϕ dependence)

$$S_{\mathrm{BH}}(\boldsymbol{k},\boldsymbol{k}') = \sum_n P_n(\cos\theta)\,\mathrm{sBH}_n\,\delta[E(\boldsymbol{k}')-E(\boldsymbol{k})] \tag{46}$$

where sBH_n are the coefficients of the Legendre polynomial expansion for the Brooks-Herring model. Then the scattering integral can be written as

$$\begin{aligned} &\int S_{\mathrm{BH}}(\boldsymbol{k}',\boldsymbol{k}) f(\boldsymbol{k}')\,d^3\boldsymbol{k}' - f(\boldsymbol{k}) \int S_{\mathrm{BH}}(\boldsymbol{k},\boldsymbol{k}')\,d^3\boldsymbol{k}' \\ &\quad = \left[\sum_{lm} \mathrm{sBH}_{lm}\, f_{lm} Y_{lm}(\theta,\phi) - \mathrm{sBH}_{0,0} \cdot \sum_{lm} f_{lm} Y_{lm}(\theta,\phi) \right] g(E) \\ &\quad = g(E) Y^T S_{\mathrm{BH}} f \end{aligned} \tag{47}$$

where S_{BH} is the net scattering matrix for the Brooks-Herring model, as shown below, up to third-order

$$S_{\mathrm{BH}} = \begin{bmatrix} 0 & 0 & 0 & 0 \\ 0 & \mathrm{sBH}_1 - \mathrm{sBH}_0 & 0 & 0 \\ 0 & 0 & \mathrm{sBH}_2 - \mathrm{sBH}_0 & 0 \\ 0 & 0 & 0 & \mathrm{sBH}_3 - \mathrm{sBH}_0 \end{bmatrix}. \tag{48}$$

For the first integral (the in-scattering term) we have used the Addition Theorem for spherical harmonics [10], whereas for the out-scattering integral the only nonzero term is from the lowest order harmonic which is isotropic. The next step is to multiply by the orthogonal spherical harmonics and integrate which yields

$$g(E) \int (Y^* Y^T S_{\mathrm{BH}} f)\,d\Omega.$$

IV. Numerics

The above Galerkin approach applies spatial and energy discretizations before introducing the spherical harmonic expansion, and therefore issues such as current conservation and the stability of the discretization must be addressed in a more general way. That is, the discretization must be appropriate for the whole system, it can not be tailored for each harmonic coefficient differential equation as in traditional approaches. The best choice of the discrete approximation to the differential operator should conserve current, be stable even on coarse meshes, and fit with the specified boundary conditions.

A. Current Conservation

The equation for the zeroth harmonic including acoustic and optical phonon and ionized impurity scattering is

$$\begin{aligned} &\frac{\partial f_{1,0}}{\partial z} - q\mathcal{E}\left(\frac{\partial f_{1,0}}{\partial E} + \frac{\gamma'}{\gamma} f_{1,0}\right) \\ &\quad = S[f_{0,0}(E), f_{0,0}(E-\Delta E), f_{0,0}(E+\Delta E)] \end{aligned} \tag{49}$$

where the scattering operator is given by

$$\begin{aligned} S[,,] = \frac{\sqrt{3}}{v(E)} c_{op}[&g^{+}(N_{op}^{+} f_{0,0}(E+\Delta E) - N_{op} f_{0,0}(E)) \\ &+ g^{-}(N_{op} f_{0,0}(E-\Delta E) - N_{op}^{+} f_{0,0}(E))] \end{aligned} \tag{50}$$

and $g^{+} = g(E+\Delta E), g^{-} = g(E-\Delta E)$ are the density of states at the appropriate energies. N_{op} is the number of optical phonons which is given by the Bose-Einstein distribution, $N_{op} = [e^{\hbar\omega_{op}/k_B T} - 1]^{-1}$ and $N_{op}^{+} = N_{op} + 1$.

In one dimension the current is only in the z-direction and is given as

$$\begin{aligned} J_z &= q \int f_{tot}(\boldsymbol{k}) v_z(\boldsymbol{k})\, d^3\boldsymbol{k} \\ &= q \int f_{tot}(\boldsymbol{k}) v(k) \cos\theta\, d^3\boldsymbol{k} \\ &\propto \int f_{1,0}(k) v(k)\, d^3\boldsymbol{k} \\ &\propto \int f_{1,0}(E) v(E) g(E)\, dE \\ &\propto \int f_{1,0}(E) \gamma(E)\, dE. \end{aligned} \tag{51}$$

The only component of the distribution function that contributes to the current in the z-direction is the $f_{1,0}$ coefficient. This of course follows from the orthogonality property of the harmonics. Using this property we can write the equation for the zeroth harmonic essentially as a current conservation equation as follows:

$$\begin{aligned} &\frac{\partial f_{1,0}}{\partial z} - q\mathcal{E}\left(\frac{\partial f_{1,0}}{\partial E} + \frac{\gamma'}{\gamma} f_{1,0}\right) \\ &\quad = S[f_{0,0}(E), f_{0,0}(E-\Delta E), f_{0,0}(E+\Delta E)] \\ &\gamma \frac{\partial f_{1,0}}{\partial z} - q\mathcal{E}\left[\gamma \frac{\partial f_{1,0}}{\partial E} + \gamma' f_{1,0}\right] \\ &\quad = \gamma S[f_{0,0}(E), f_{0,0}(E-\Delta E), f_{0,0}(E+\Delta E)] \\ &\int \frac{\partial(\gamma f_{1,0})}{\partial z}\, dE - q\mathcal{E} \int \left[\frac{\partial(\gamma f_{1,0})}{\partial E}\right] dE \\ &\quad = \int \gamma(E) S[f_{0,0}(E), f_{0,0}(E-\Delta E), \\ &\qquad f_{0,0}(E+\Delta E)]\, dE \\ &\int \frac{\partial(\gamma f_{1,0})}{\partial z}\, dE \\ &\quad = q\mathcal{E}[\gamma(E) f_{1,0}]_0^\infty \\ &\qquad + \int \gamma(E) S[f_{0,0}(E), f_{0,0}(E-\Delta E), \\ &\qquad f_{0,0}(E+\Delta E)]\, dE. \end{aligned} \tag{52}$$

In the last equation above, the left-hand side is proportional to the spatial derivative of the current, which follows from (51), and therefore must be zero if current is to be conserved. Using the boundary condition that $\gamma(E) f_{1,0} \to 0$ as $E \to \infty$, which follows from the assumption that the total distribution approaches zero "faster" than any polynomial function of energy, the first term is zero. Hence, the integral of the scattering term over energy must reduce to zero for current to be conserved. From the scattering operator given in (50), it can be easily shown that this condition is satisfied.

Thus, current conservation is inherent in the continuous case and the discretized equation should preserve this property. To see how this constrains the discretization method, consider the time varying Boltzmann equation in one real-space dimension

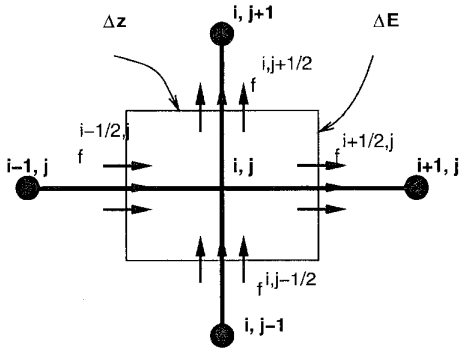

Fig. 4. Control volume for energy-space discretization.

which, after expansion into spherical harmonics, is

$$\begin{aligned} &\frac{1}{v(E)} \frac{\partial f}{\partial t} + \frac{\partial(Gf)}{\partial z} - q\mathcal{E}(z) \frac{\partial(Gf)}{\partial E} + q \frac{\mathcal{E}(z)\gamma'}{2\gamma} Hf \\ &\quad = \frac{1}{v(E)} \left(\frac{\partial f}{\partial t}\right)_c. \end{aligned} \tag{53}$$

Discretizing (53) using a box scheme with mesh spacing Δz in space and ΔE in energy ($\Delta A = \Delta z \Delta E$) yields

$$\begin{aligned} &\frac{\Delta A}{v^j} \frac{\partial f}{\partial t} + \Delta E G(f^{i+1/2,j} - f^{i-1/2,j}) \\ &\quad - q\Delta z \mathcal{E}^i G(f^{i,j+1/2} - f^{i,j-1/2}) \\ &\quad + q\Delta A \frac{\mathcal{E}^i \gamma'^j}{2\gamma^j} H f^{i,j} = \frac{\Delta A}{v^j} \left(\frac{\partial f_{i,j}}{\partial t}\right)_c. \end{aligned} \tag{54}$$

The terms $f^{i+1/2,j}, f^{i-1/2,j}, f^{i,j+1/2}, f^{i,j-1/2}$ represent the average 'flux' at the interface of the control volume as shown in Fig. 4.

As is easily shown, using the control volume and interface flux approach will insure current conservation by insuring invariance in space of the integral of $f_{1,0}$ over energy. But to completely specify the discretization method it is necessary to choose a representation of the 'average' flux at the interface in terms of quantities at the mesh points. For example, one approach is to everywhere use a simple two-point discretization for the flux, $f^{i+1/2,j} = f^{i,j}$ and $f^{i-1/2,j} = f^{i-1,j}$ and similarly for the flux in the direction of the energy axis. In the next section, we show that issues of stability determine exactly which representations are best.

B. Upwinded Discretization

When determining expressions for the flux in terms of mesh quantities, it must be remembered that the flux here is a vector quantity and therefore there exists the added freedom of choosing a different expression for each component of the flux vector. Hence, a large number of variations are possible even for a two point discretization scheme when two dimensions and a few orders (the size of the flux vector) are included. Using trial and error, a first-order discretization that was usually effective was found, which is denoted as a one-sided discretization in the following discussion. This scheme uses a forward one-sided, two-point approximation to the derivatives in space and energy

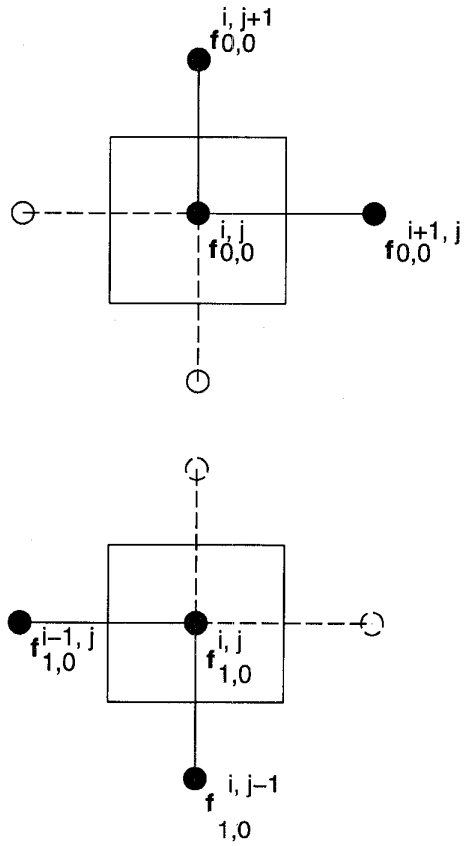

Fig. 5. The one-sided discretization scheme, where the horizontal axis represents real space and the vertical direction energy. The index i corresponds to discretization in space and the index j to discretization in energy.

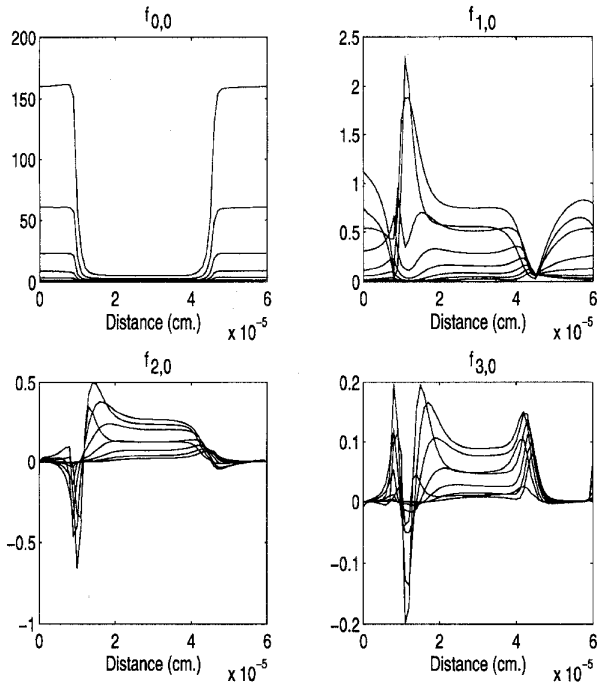

Fig. 6. Stable results for the spherical harmonic coefficients (in arbitrary units) using the discretization shown in Fig. 5 for the simulation of an n^+nn^+ structure.

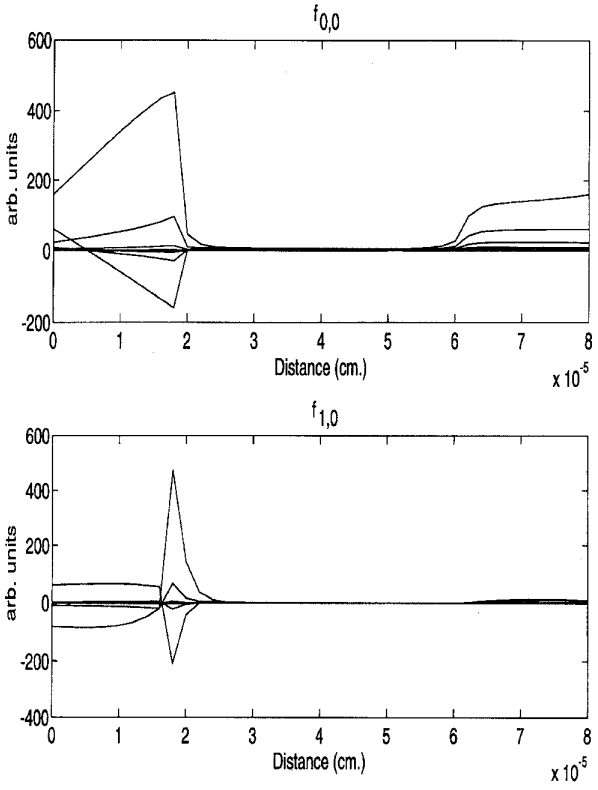

Fig. 7. Unstable results for one-sided scheme.

of the coefficients of even harmonics $f_{0,0}, f_{2,0}$ etc. and a backward one-sided, two-point approximation in space and energy to the derivatives of the odd harmonics $f_{1,0}, f_{3,0}$ etc. This method is shown schematically in Fig. 5, and the results obtained up to third-order using this method are shown in Fig. 6.

Although this discretization scheme is successful in most cases, under certain circumstances it became unstable, for example near the n^+n junction in the simulation of the n^+nn^+ diode [12]. An example of the instability is shown in Fig. 7. In this figure the coefficients are plotted as a function of space, but the oscillations are not in space, they are in energy in the region to the left of the n^+n junction. The salient fact about this junction is that this is the only part of the device where the electric field is positive for the bias conditions shown in Fig. 7. We also know that the discretization shown in Fig. 5 is stable for a homogeneous field only if it is negative everywhere but not if it is positive. These two observations clearly imply that the sign of the field is the key to stable discretization. To better understand the stability issues we will use the insights from the 1-D wave equation and use it to guide our approach.

In the time dependent case, the Boltzmann equation is a hyperbolic equation (a wave equation). It is well known that if the wave equation (in one-dimension)

$$U_t + aU_x = 0 \tag{55}$$

is discretized using a forward Euler time marching scheme as shown below:

$$U_i^{k+1} - U_i^k = \frac{\Delta t}{\Delta x} a(U_{i+1/2}^k - U_{i-1/2}^k) \tag{56}$$

where k is the index for temporal discretization and i for

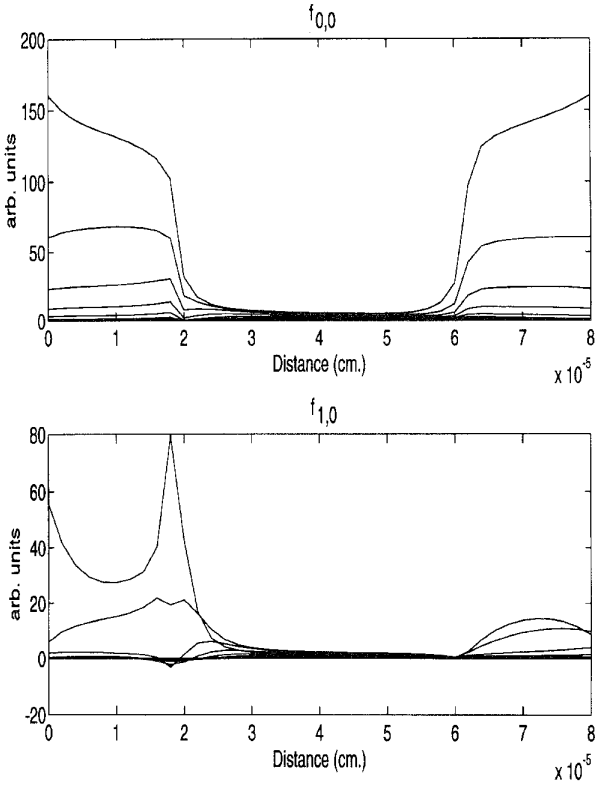

Fig. 8. Stable results using upwinded scheme.

spatial discretization, then for a stable discretization the spatial derivative must be done either in the forward or the backward direction depending on the sign of the velocity a [13]. This is know as upwind differencing. Thus, upwind differencing requires that

$$a<0 \rightarrow U_i^{k+1} - U_i^k = \frac{\Delta t}{\Delta x} a(U_{i+1}^k - U_i^k) \tag{57}$$

$$a>0 \rightarrow U_i^{k+1} - U_i^k = \frac{\Delta t}{\Delta x} a(U_i^k - U_{i-1}^k). \tag{58}$$

Note that in the control volume sense the above equation simply conserves the flux, that is if there is a net flux leaving a control volume in space then at the next time step the value of the function at the center of that control volume is reduced commensurately. Of course the change can be an increase or a decrease depending on the sign of the net flux.

In the Boltzmann equation, the energy derivative has a coefficient which changes sign depending on the electric field and therefore it is the energy derivative that must be "winded". Now, up to first-order the flux term in energy is given by Gf where

$$G = \begin{bmatrix} 0 & \frac{1}{\sqrt{3}} \\ \frac{1}{\sqrt{3}} & 0 \end{bmatrix} \quad Gf = \begin{bmatrix} \frac{1}{\sqrt{3}} f_{1,0} \\ \frac{1}{\sqrt{3}} f_{0,0} \end{bmatrix}.$$

Therefore, the flux difference in energy has two possible

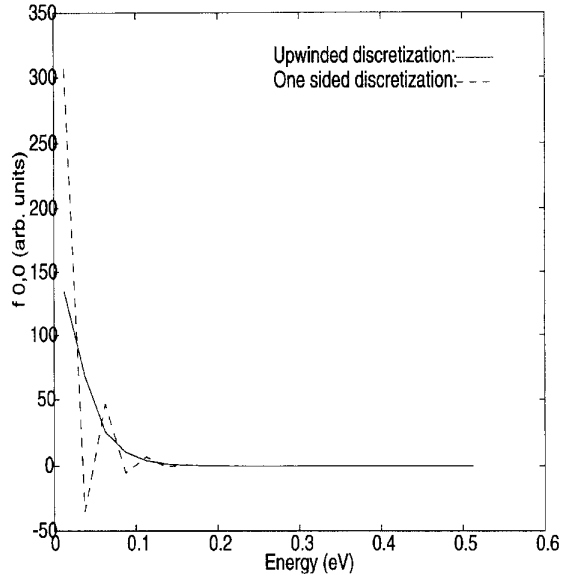

Fig. 9. A comparison of the solution for $f_{0,0}$ obtained using the one-sided (dash) and upwinded (solid) discretization schemes.

expressions: if the electric field is negative it is

$$(-\mathcal{E}^i)\begin{bmatrix} f_{1,0}^j - f_{1,0}^{j-1} \\ f_{0,0}^{j+1} - f_{0,0}^j \end{bmatrix}$$

otherwise it is

$$\mathcal{E}^i\begin{bmatrix} f_{1,0}^{j+1} - f_{1,0}^j \\ f_{0,0}^j - f_{0,0}^{j-1} \end{bmatrix}$$

where we have suppressed the $1/\sqrt{3}$ factor for clarity. Note that the direction of the two point discretization for the even and odd harmonics are still opposite to each other as in the one-sided discretization but these directions flip sign depending on the electric field direction.

The results obtained using the upwinded discretization for the same bias conditions as in Fig. 7 are shown in Fig. 8. Clearly the unstable oscillations introduced due to the discretization have been suppressed here. The advantage of using the more stable winded method is most clearly seen if $f_{0,0}$ is plotted as a function of energy in the left n^+ region in the two cases (Fig. 9).

An upwind scheme was also used in [14] where the BTE was solved by direct discretization of the distribution function in spherical coordinates but without using an expansion in spherical harmonics.

It is worth noting that the extensions of this scheme to two real-space dimensions is not trivial, first because the discretized variable is a vector and secondly the choice of the direction of the winding is more complex in two dimensions [15], [16].

C. Boundary Conditions

The Boltzmann equation has only first-order derivatives in space whereas physically we would like to specify the boundaries (Ohmic contacts for example) in space at both the left and right end points. This seeming inconsistency can

be resolved by using the fact that the Boltzmann equation expansion in spherical harmonics is really a set of equations. Thus, we specify the zeroth-order harmonic at both edges but leave the first-order coefficient unspecified everywhere. In general all even harmonics are fixed on both sides and all odd harmonics are left floating at the edges and their values calculated everywhere. We set the zeroth-order harmonic to be the Maxwellian at the lattice temperature and the second and higher harmonics to zero. For low-order spherical harmonics these boundary conditions have a physical interpretation: specifying the zeroth- and second-order harmonics, and solving for the first and third is equivalent to specifying the electron concentration and the electron temperature on both edges but solving for the electron current and the heat flux at those points.

In the energy direction we assume that all harmonics are zero beyond some maximum energy and also for the odd harmonics use the fact that the odd harmonics must be zero at zero energy. This is a necessary condition for the odd harmonics otherwise there would be a discontinuity in the distribution at zero energy. This can be demonstrated for the first-order harmonic term $f_{1,0}(k)\cos\theta$ by considering the distribution along the k_z axis—for $k_z > 0, \cos\theta = 1$ but for $k_z < 0, \cos\theta = -1$. Therefore if $f_{1,0}$ has a nonzero value in the neighborhood of $k_z = 0$ then the distribution would have a discontinuity at $k_z = 0$.

D. Self-Consistent Solution with Poisson's Equation

In all the discussion up to now we have assumed that the electric field was known or given independently. Of course, in general the electric potential or field has to be solved self-consistently with the distribution function. Thus, along with the Boltzmann equation we need to discretize and solve Poisson's equation. Using the box-discretization method mentioned earlier it is fairly straightforward to set up the discretized Poisson's equation. The only complication comes about from the fact that in the self-consistent formulation the system of equations becomes nonlinear: the electric field multiplies the energy derivative of the distribution function coefficients. Hence, this nonlinear system must be solved.

A standard way of solving nonlinear systems is Newton's method, which is known to converge quadratically [17]. Therefore if a good initial guess is known, after typically five to eight iterations, the solution is found. The size of the matrix problem increases only slightly as there is only one extra unknown at each real space point (there may be 50 coefficients in energy at each point) but the cost in the number of iterations is of course significant. Also the sparsity of the matrix is reduced slightly because there are many nonzero entries associated with the extra unknown (as shown below) for a typical Jacobian matrix, where the P matrix blocks are the coefficients in the discrete approximation to the integral of f_{lm} over energy which gives the electron concentration at that point in real space. Using this method, we have found no difficulty in converging from the zero potential inital guess.

An alternate method of solving the nonlinear system is to iteratively solve the Boltzmann and Poisson equations [18], though the convergence of such a scheme is not assured. Nonetheless in multiple real space dimensions such an iterative method may be preferred as the sparsity of the discretization matrix is degraded more severely in multiple dimensions by the inclusion of Poisson's equation [19].

V. Simulation Results

In this section we present results using the arbitrary order expansion method described in the previous sections. We will first present results for the homogeneous problem with no spatial variation and compare those results with bulk Monte Carlo data which is a test of the implementation of our scattering terms. Then results for 1-D structures such as uniform doping and n^+nn^+ diode are presented. All the results presented are using a self-consistent scheme and were obtained using a direct sparse solver on the sparse matrix generated by the Galerkin method.

The physical model consisting of the band structure and the scattering mechanisms are kept simple yet sufficiently rich to provide real physical insight. The basic theory allows for the use of more complex physical models such as nonparabolic bands or multiple bands [20].

For the inhomogeneous simulations described below the spatial discretization was usually 50–60 mesh lines and the energy discretization was usually from 0 to 1 eV with 25 meV steps. The computational complexity is therefore the same as solving a 2000–3000 unknown sparse matrix problem for each Newton step. The number of Newton steps needed to meet the termination criterion, based on the norm of the residue, was less than 10.

$$
\begin{bmatrix}
\ddots & \ddots & & \ddots & & & & \mathbf{0} \\
 & W_1^{i,j} & W_2^{i,j} & & W_3^{i,j} & & & \\
 & & W_1^{i+1,j} & W_2^{i+1,j} & & W_3^{i+1,j} & & \\
 & & \ddots & \ddots & & & & \ddots \\
P & \dots & P & 1 & -2 & 1 & 0 & \\
 & P & \dots & 0 & 1 & -2 & 1 &
\end{bmatrix}
\begin{bmatrix}
\vdots \\
\delta f^{i,j} \\
\delta f^{i+1,j} \\
\vdots \\
\delta f^{i,j+1} \\
\delta f^{i+1,j+1} \\
\vdots \\
\delta \psi^{i,j} \\
\delta \psi^{i+1,j} \\
\vdots
\end{bmatrix}
$$

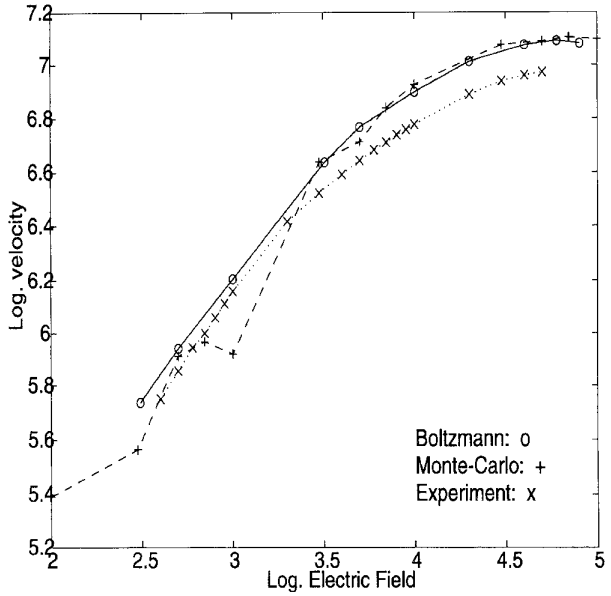

Fig. 10. Mean electron velocity in the bulk for undoped silicon as a function of the electric field calculated using the spherical harmonic expansion method and a Monte Carlo method along with experimental data.

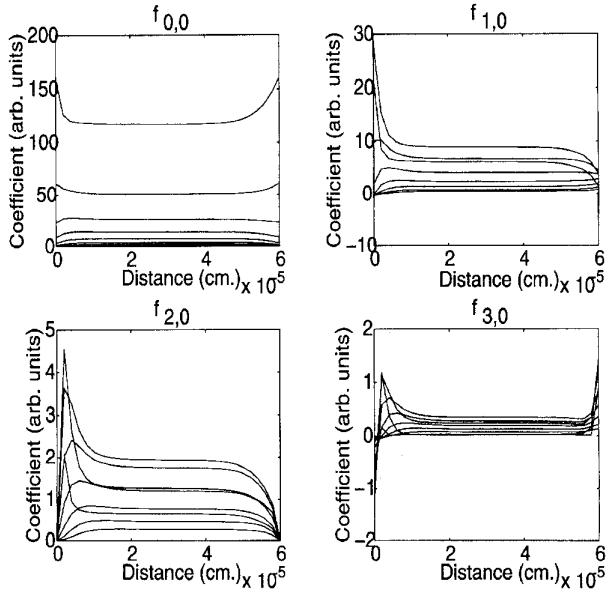

Fig. 11. The potential, electric field, normalized electron concentration and the normalized current for a resistor obtained from the Boltzmann equation solution up to third-order.

A. Homogeneous Problem

Here we set all spatial derivatives to zero and then solve for the coefficients. Using results up to first-order we can match the distribution function obtained from Monte Carlo simulations [21] if the same scattering mechanisms and band structure are used. In Fig. 10 the electron mean velocity calculated using the spherical harmonic approach and the Monte Carlo method is plotted as a function of the applied electric field along with experimental data. The graph clearly demonstrates that the results from the spherical harmonic

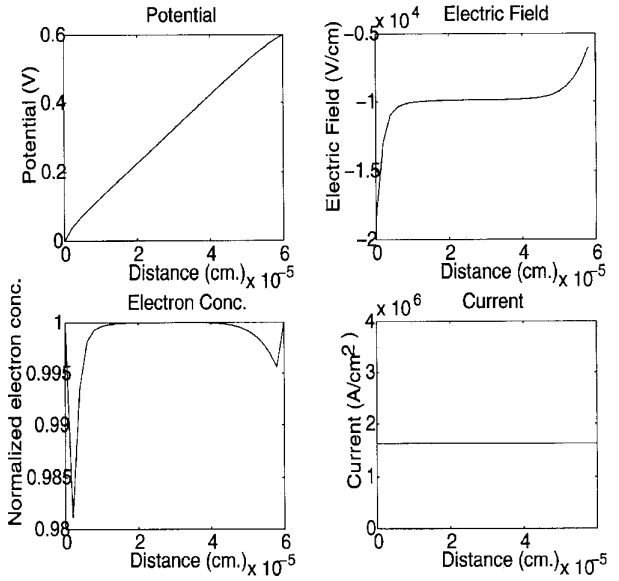

Fig. 12. Zero to third order coefficients as a function of position for different electron energies (starting from 25 meV with 25 meV spacing in energy) for the 0.6 μm resistor shown in the previous figure.

method and Monte Carlo are essentially the same except for the noise in the Monte Carlo data. The experimental data is qualitatively similar but the saturation velocity is about 20% lower because of the simplistic band and scattering model used in the simulation.

B. Resistor

If we simulate a uniformly doped finite region of silicon (a resistor) with an applied bias, we expect to see a uniform field in the bulk and some carrier heating if the field is large enough. Figs. 11 and 12 show the first four coefficients and the macroscopic parameters obtained from such a simulation with an average field of 1×10^4 V/cm. There are a number of noteworthy features even in this simplest inhomogeneous problem.

1) The magnitude of the coefficients in the uniform part of the resistor decreases monotonically as the order is increased.
2) The electron temperature in the bulk of the resistor is above the lattice temperature as evinced by the compression of the lines of $f_{0,0}$ at the different energies at the center as compared to the edges. The magnitude of $f_{0,0}$ decreases faster at the edges than at the center as a function of energy which is equivalent to having a lower electron temperature at the edges than the center.
3) There is a small charge buildup near both the left and right contacts. This occurs because at the contacts we have assumed that the isotropic part of the distribution ($f_{0,0}$) is a Maxwellian at the lattice temperature, whereas in the center of the resistor the electron gas is at an elevated temperature. Thus, there would be an excess thermal current if the field were uniform all the way up to the contacts. Hence, to maintain a constant current the electric field deviates from its value in the bulk to counteract these thermal currents.

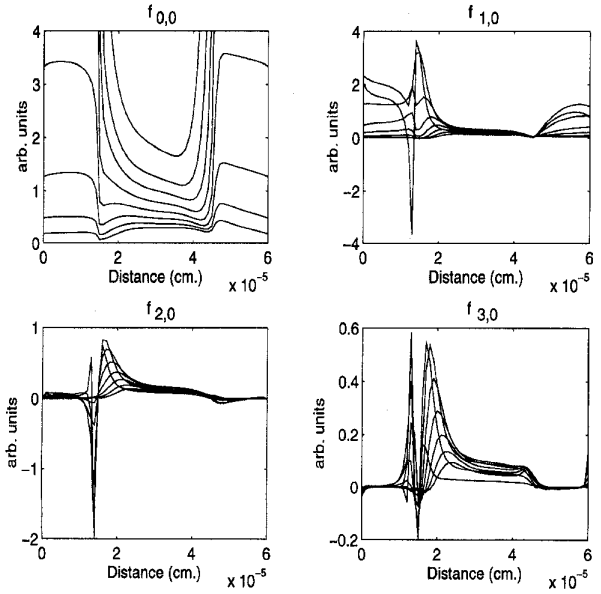

Fig. 13. Spherical harmonic coefficients for a 0.6 μm n^+nn^+ diode with a doping of 2×10^{18} cm^{-3} and 1×10^{17} cm^{-3} in the n^+ and n regions and a bias of 0.8 V. The coefficients are for different energies starting from 25 meV with 25 meV spacing in energy.

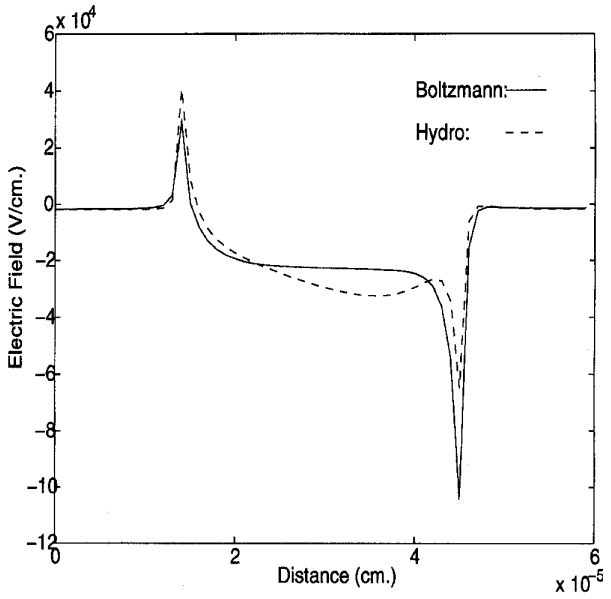

Fig. 15. A comparison of the electric field computed from the solution of the Boltzmann and Poisson's equations with that obtained from the hydrodynamic model for a 0.6 μm n^+nn^+ diode with a doping of 2×10^{18}cm^{-3} and 1×10^{17} cm^{-3} in the n^+ and n regions and a bias of 0.8 V.

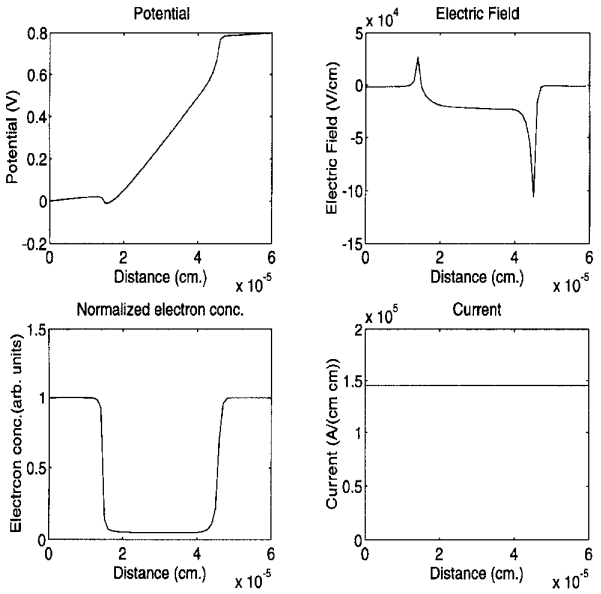

Fig. 14. Average quantities for a 0.6 μm n^+nn^+ diode with a doping of 2×10^{18} cm^{-3} and $1 \times 10^{17} cm^{-3}$ in the n^+ and n regions and a bias of 0.8 V.

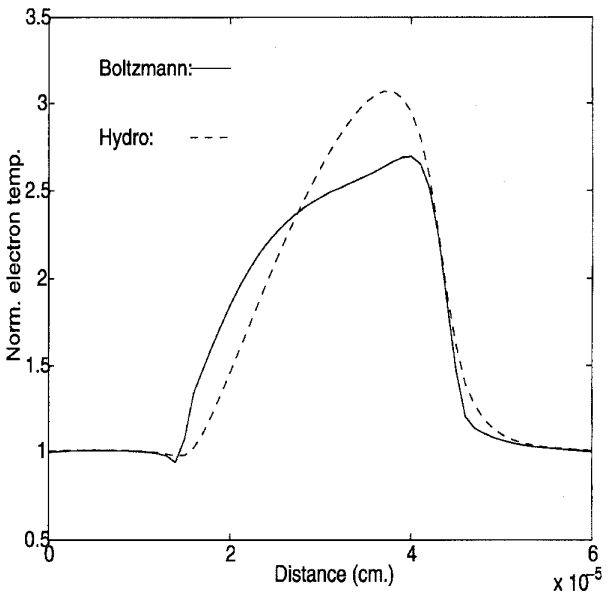

Fig. 16. A comparison of the electron temperature computed from the solution of the Boltzmann and Poisson's equations that obtained from the hydrodynamic model for a 0.6 μm n^+nn^+ diode with a doping of 2×10^{18} cm^{-3} and 1×10^{17} cm^{-3} in the n^+ and n regions and a bias of 0.8 V.

4) The current is constant as was predicted in Section IV-D, using the discretization methods described earlier.

C. Diode

Fig. 13 shows the computed spherical harmonics coefficients for an n^+nn^+ diode as a function of position at different energy values (separated by 25 meV). The electron concentration and the current obtained from the calculated distribution function along with the potential and electric field obtained by the self-consistent solution of Poisson's equation for the same device are shown Fig. 14.

A comparison between the electric field and electron temperature obtained using the hydrodynamic model [22] and the solution of the Boltzmann equation for this particular structure is shown in Figs. 15 and 16. Although the field and temperature obtained using the two approaches are not identical because the mobility model used in the hydrodynamic corresponds to slightly different scattering parameters than

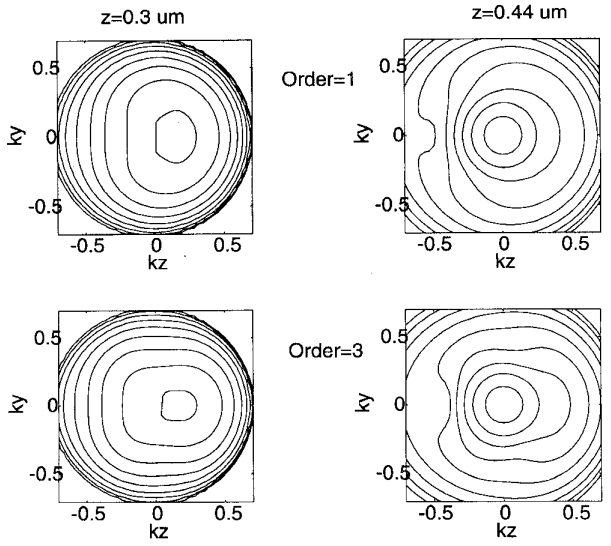

Fig. 17. Contours of constant distribution function (separated by 3x) over a normalized k_z, k_y plane for the device of Fig. 13. The figures on the left are at $z = 0.3$ μm and the figures on the right are at $z = 0.44$ μm, including the first- (top) and third-order harmonic expansions (bottom).

those used in the Boltzmann solver, the results are comparable. Note also that the peak electric field obtained from the Boltzmann solution is higher than that from the macroscopic hydrodynamic model as was reported in [18].

In Fig. 17 the distribution functions obtained using different orders of spherical harmonics are compared at two points along the diode. The impact of including higher orders is obvious as it tends to produce a more streamed distribution than if only the first two orders were considered. The electron temperatures obtained in the two cases are quite close, demonstrating the insensitivity of temperature to details of the distribution. The coefficients of the distribution as a function of the energy at two positions along the diode are shown in Fig. 18. Note that the distribution at the peak electric field point ($z = 0.44$ μm) shows the mixing of two carrier populations: hot carriers from the source and cold carriers from the drain. This can be deduced by examining the two slopes evident in the isotropic part of the distribution ($f_{0,0}$): the larger slope (lower temperature) up to 0.1 eV is due to cold carriers from the drain and the smaller slope (higher temperature) beyond 0.1 eV is due to hot carriers from the source. This example also demonstrates the difficulty any averaging scheme (such as a moments method) would have in correctly estimating the hot carrier population. For instance, the average temperature at $z = 0.44$ μm is almost equal to the lattice temperature (as shown in Fig. 15) because most of the electrons are cold electrons from the drain. Nevertheless, there is a substantial number of hot carriers present, as can be seen in Fig. 18.

VI. Conclusion

We have presented a Galerkin method that allows the use of an arbitrary order spherical harmonic expansion for the solution of the space-dependent coupled Poisson-Boltzmann equation. The specific Galerkin method used allows the number of spherical harmonics considered to be essentially a

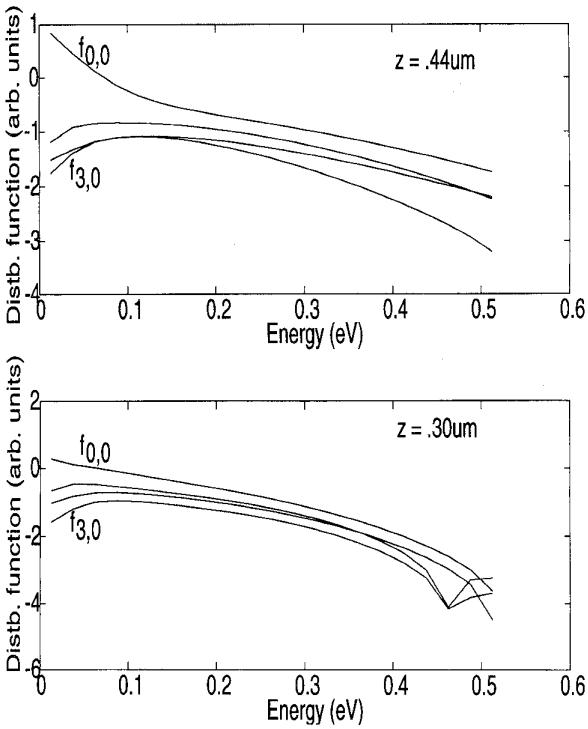

Fig. 18. Logarithm of the coefficients of spherical harmonics up to third order for the 0.6 μm n^+nn^+ diode at 0.8 V shown in the preceding figures at $z = 0.44$ μm and $z = 0.30\mu$m.

program parameter, and thus facilitates an examination of the impact of higher order effects on device behavior. Simulation results, up to third order, based on the Galerkin method for 1-D structures were presented. From the simulations results obtained by self-consistently solving Poisson's equation it was demonstrated that spherical harmonic coefficients beyond the the first can be significant, and neglecting them may not be appropriate in certain cases. Also it was shown that under high and rapidly varying fields the calculated distribution function can differ significantly from a displaced Maxwellian or other simple form and therefore any macroscopic method will perform poorly at estimating the details of the distribution function. Preliminiary work in two-real space dimensions [19] has shown that the Galerkin method can be extended to multiple real space dimensions.

Appendix

The Physical Model

For the simulation results presented in this and subsequent chapters the following scattering mechanisms and band structure are used.

Band Model

A single parabolic band with an effective mass of 0.26 times the electron mass is assumed

$$E = \frac{\hbar^2 k^2}{2m^*}$$

Acoustic Phonon Scattering

The scattering probability for an electron starting from an initial momentum state k to the state k' under acoustic phonon scattering is [11]

$$P(\boldsymbol{k},\boldsymbol{k}') = \frac{2\pi k_B T_0}{\hbar V u_l^2 \rho}\mathcal{E}_1^2 \delta[E(\boldsymbol{k}') - E(\boldsymbol{k})] \tag{59}$$

where V is the volume, u_l^2 is the sound speed in silicon, ρ is the density of silicon, $\mathcal{E}_1$ is the deformation potential for the lattice. As we are working in energy space we need to convert the above scattering probability from momentum space to energy space which is done by integrating over the 3-D $\boldsymbol{k}$ space after appropriate scaling

$$\frac{V}{(2\pi)^3}4\pi \int P(E(k),E(k'))k'^2\,dk' = \frac{V}{2\pi^2}\frac{\sqrt{2}m^{*^{3/2}}}{\hbar^3}\int P(E,E')E'^{1/2}\,dE'. \tag{60}$$

Hence, the acoustic scattering rate becomes

$$P(E,E') = \frac{2^{1/2}m^{*^{3/2}}k_B T_0}{\pi\hbar^4 u_l^2 \rho}\mathcal{E}_1^2\delta[E-E']E^{1/2}. \tag{61}$$

The values of the parameters used are

m^*	$0.26\,\mathrm{m_0}$
u_l	$9.00\times10^3\,\mathrm{ms^{-1}}$
ρ	$2.33\times10^3\,\mathrm{kg\,m^{-3}}$
$\mathcal{E}_1$	$9.00\,\mathrm{eV}$

Optical Phonon Scattering

For optical phonons the scattering rate is:

$$P(\boldsymbol{k},\boldsymbol{k}') = \frac{\pi(D_tK)^2}{V\rho\omega_{op}}\{N_{op};N_{op}+1\}\delta[E(\boldsymbol{k}')-E(\boldsymbol{k})\mp\hbar\omega] \tag{62}$$

where D_tK is the coupling constant, ω_{op} is the frequency of the optical phonon and N_{op} is the number of optical phonons using Bose statistics. Note that N_{op} is associated with $-\hbar\omega$ and $N_{op}+1$ is associated with the $+\hbar\omega$ for the cases of absorption and emission of optical phonons.

The above probability can be written in energy space to yield

$$P(E,E') = \frac{(D_tK)^2}{\rho\omega_{op}}\frac{m^{*^{3/2}}}{\sqrt{2}\pi\hbar^3}\{N_{op};N_{op}+1\}E^{1/2}\cdot\delta[E'-E\mp\hbar\omega]. \tag{63}$$

The parameter values used in the above equation are

D_tK	$5.0\times10^8\,\mathrm{eV\,cm^{-1}}$
$\hbar\omega_{op}$	$50\,\mathrm{meV}$

Ionized Impurity Scattering

For ionized impurity scattering we use the Brooks-Herring model which is based on assuming a shielded potential (the Yukawa potential) for the ionized impurity. The resulting scattering probability is given as

$$S(\boldsymbol{k},\boldsymbol{k}') = \frac{Z^2q^4}{\epsilon_{Si}^2\hbar}N_i\frac{1}{[\beta^2+2k^2(1-\cos\theta)]^2}\cdot\delta[E(\boldsymbol{k}')-E(\boldsymbol{k})] \tag{64}$$

where Z is the ordinality of the impurity charge, N_i is the impurity concentration, β is the Debye length and θ is the angle between the k and k' vectors.

ACKNOWLEDGMENT

The authors would like to thank Dr. J. Jacobs for his help in understanding the hydrodynamic model, and to acknowledge Dr. K. Nabors' help with the spherical harmonic identities. In addition, we would like to thank Prof. A. Henning of Dartmouth College for valuable discussions and for providing the Monte Carlo simulation results. Finally, we would like to thank the anonymous reviewers for their helpful comments.

REFERENCES

[1] H. D. Rees, "Numerical solution of electron motion in solids," *J. Phys. C: Solid State Phys.*, vol. 5, pp. 641–656, 1972.

[2] R. W. Hockney, R. A. Warriner, and M. Reiser, "Two-dimensional particle models in semiconductor-device analysis," *Electron. Lett*, vol. 10, pp. 484–486, 1974.

[3] Y. L. Le Coz, "Semiconductor device simulation: A spectral method for solution of the Boltzmann Transport Equation," Ph.D. dissertation, Mass. Inst. Technol., 1988.

[4] E. M. Conwell and M. O. Vassell, "High-field transport in n-type GaAs," *Phys. Rev.*, vol. 166, no. 3, pp. 797–821, 1968.

[5] T. Iizuka and M. Fukuma, "Carrier transport simulator for silicon based on carrier distribution function evolutions," *Solid State Electron.*, vol. 33, pp. 27–34, 1990.

[6] N. Goldsman, L. Hendrickson, and J. Frey, "A physics-based analytical/numerical solution to the Boltzmann transport equation for use in device simulation," *Solid State Electron.*, vol. 34, pp. 389–396, 1991.

[7] A. Gnudi, D. Ventura, and G. Baccarani, "One-dimensional simulation of a bipolar transistor by means of spherical harmonics expansion of the Boltzmann equation," in *Proc. SISDEP Conf*, 1991, pp. 205–208.

[8] K. A. Hennacy, Y.-J. Yu, N. Goldsman, and I. D. Mayergoyz, "Deterministic MOSFET simulation using a generalized spherical harmonic expansion of the Boltzmann equation," *Solid State Electron.*, vol. 38, pp. 1485–1495, 1995.

[9] D. Ventura, A. Gnudi, G. Baccarani, and F. Odeh, "Multidimensional spherical harmonics expansion of Boltzmann Equation for transport in semiconductors," *Appl. Math. Lett*, vol. 5, no. 3, pp. 85, 1992.

[10] G. Sansone, *Orthogonal Functions*. New York: Intersci., 1959.

[11] C. Jacoboni and L. Reggiani, "The Monte Carlo method for the solution of charge transport in semiconductors with applications to covalent materials," *Rev. Modern Phys.*, vol. 55, no. 3, pp. 645–704, 1983.

[12] K. Rahmat, J. White, and D. A. Antoniadis, "A Galerkin method for the arbitrary order expansion in momentum space of the Boltzmann equation using spherical harmonics," in *Proc. NUPAD V*, 1994, pp. 133–136.

[13] R. D. Richtmeyer and K. W. Morton, *Difference Methods for Initial-Value Problems*. New York: Intersci., 1967.

[14] E. Fatemi and F. Odeh, "Upwind finite difference solution of Boltzmann equation applied to electron transport in semiconductor devices," *J. Computat. Phys.*, vol. 108, pp. 209–217, 1993.

[15] P. L. Roe, "Approximate Riemann solvers, parameter vectors, and difference schemes," *J. Computat. Phys.*, vol. 43, pp. 357–372, 1981.

[16] M. Y. Hussaini, A. Kumar, and M. D. Salas, Eds., *Algorithmic Trends in Computational Fluid Dynamics*. New York: Springer-Verlag, 1991, pp. 341–395,

[17] J. M. Ortega and W. C. Rheinholdt, *Iterative solution of Nonlinear Equations in Several Variables*. New York: Academic, 1970.

[18] H. Lin, N. Goldsman, and I. D. Mayergoyz, "Device modeling by deterministic self-consistent solution of Poisson and Boltzmann transport equations," *Solid State Electron.*, vol. 35, pp. 769–778, 1992.
[19] K. Rahmat, J. White, and D. A. Antoniadis, "Solution of the Boltzmann Transport Equation in two real space dimensions using a spherical harmonic expansion in momentum space," in *IEDM Tech. Dig.*, 1994, pp. 359–362.
[20] A. Gnudi, D. Ventura, and G. Baccarani, "Modeling impact ionization in a BJT by means of a spherical harmonic expansion of the Boltzmann Transport Equation," *IEEE Trans. Computer-Aided Design*, vol. 12, pp. 1706–1713, 1993.
[21] A. Henning, private communication.
[22] K. Rahmat, J. White, and D. A. Antoniadis, "Computation of drain and substrate currents in ultra-short NMOSFET's using the hydrodynamic model," *IEEE Trans. Computer-Aided Design*, vol. 12, pp. 817–824, 1993.

Khalid Rahmat (S'85–M'95) received the B.S. and M.S. degrees in electrical engineering and computer science from the Massachusetts Institute of Technology, Cambridge, in 1984 and 1986, respectively.

From 1986 to 1989 he was with Standard Microsystems Corp., NY in the process development group. In 1989 he returned to M.I.T. to pursue the doctoral degree in the area of semiconductor device simulation, and received the Ph.D. degree in 1995. Since then he has been with the ULSI Research Laboratory within Hewlett-Packard Labs. His current research interests are focused on device and interconnect modeling and optimization.

Jacob White (S'80–M'83) received the B.S. degree in electrical engineering and computer science from the Massachusetts Institute of Technology, Cambridge, and the S.M. and Ph.D. degrees in electrical engineering and computer science from the University of California, Berkeley.

He was with the IBM T. J. Watson Research Center from 1985 to 1987. He was the Analog Devices Career Development Assistant Professor at the Massachusetts Institute of Technology from 1987 to 1989, and was a 1988 Presidential Young Investigator. He is currently an Associate Professor at M.I.T. and a former Associate Editor for the IEEE TRANSACTIONS ON COMPUTER-AIDED DESIGN. His current research interests are in serial and parallel numerical algorithms for problems in circuit, interconnect, device, and microelectromechanical system design.

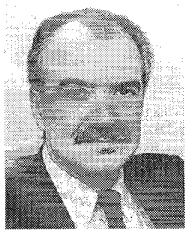

Dimitri A. Antoniadis (M'79–SM'83–F'90) received the B.S. degree in physics from the National University of Athens, Greece, in 1970 and the M.S.E.E. and Ph.D. degrees in electrical engineering from Stanford University, Stanford, CA, in 1973 and 1976, respectively.

From 1969 to 1976, he conducted research in the area of measurements and modeling of the earth's ionosphere and thermosphere. Starting with the SUPREM process simulator in 1976, his technical activity has been in the area of semiconductor devices and integrated curcuit technology. From 1976 to 1978, he was Research Associate and Instructor, Department of Electrical Engineering, Stanford University. In 1978, he joined the Massachusetts Institute of Technology, Cambridge, where he is Professor of Electrical Engineering. Currently, he is Director of the SRC Center of Excellence for Microsystem Technologies, MIT. He is the author and coauthor of more than 150 technical articles.